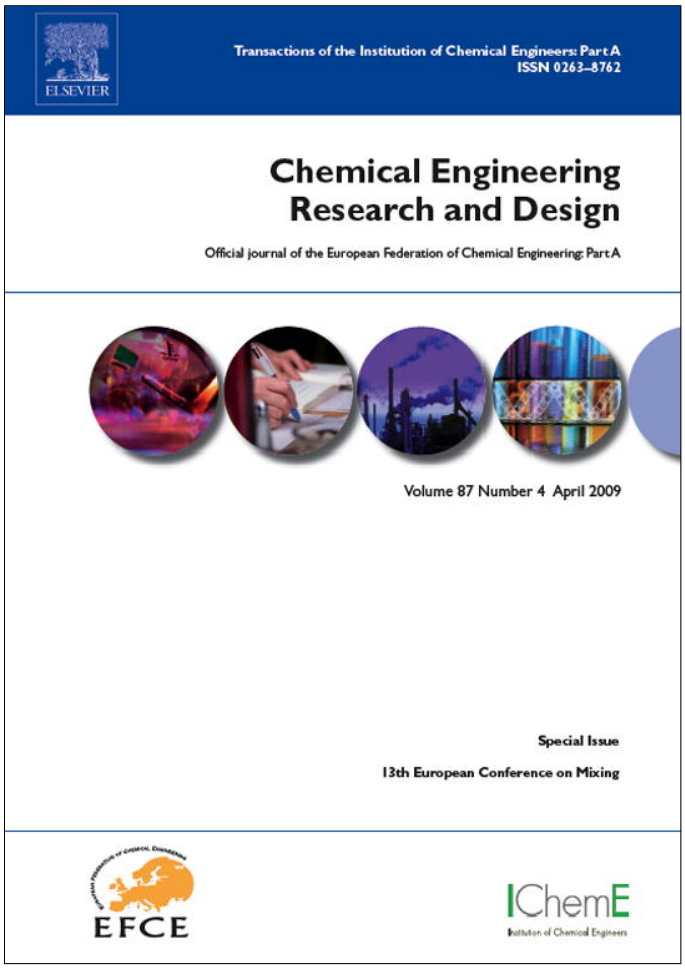

CHEMICAL ENGINEERING RESEARCH AND DESIGN 87 (2009) 550–556

Contents lists available at ScienceDirect

Chemical Engineering Research and Design

journal homepage: www.elsevier.com/locate/cherd

Scalar mixing with fixed and fluidized particles in micro-reactors

J.J. Derksen

Chemical & Materials Engineering Department, University of Alberta, Edmonton, Alberta, T6G 2G6 Canada

ABSTRACT

We study by means of direct numerical simulation the mixing performance of fixed and fluidized beds of spherical, monodisperse particles in narrow channels. Mixing performance is being characterized by an effective diffusion coefficient. The Reynolds numbers based on the channel width and superficial velocity are of the order of 10. Under these laminar conditions the mixing of a passive scalar is greatly enhanced by the presence of particles, with mobile particles (in fluidized beds) performing much better than fixed particles. The simulations allow for the design of micro-scale mixing devices in terms of reactor size (length and width), particle size, solids volume fraction, and flow rate.

Keywords: Micro-reactor; Scalar mixing; Fluidization; Laminar flow

1. Introduction

For many (chemical) engineering applications, specifically for those involving heat and mass transfer over solid surfaces, micro-fluidic devices form an interesting alternative. Micro-reactors can integrate various functions in compact volumes, they can be used for efficient chemical and (bio)medical diagnostics, and for onboard applications (e.g. fuel cells in portable equipment). Particle formation and handling is an important application of micro-reactors. Examples are (nano)crystallization processes in impinging jet reactors (Johnson and Prud'homme, 2003), or in T or Y mixers (Roelands et al., 2003). Also particles coating processes have been carried out in micro-reactors (Andersson et al., 2000).

Scalar mixing in micro-reactors is a notoriously difficult issue. The often laminar flow requires specific active or passive mixing devices to homogenize initially separate process streams (Djenida and Moghtaderi, 2006). In this paper we investigate how the presence of particles may contribute to scalar mixing. More specifically we compare the mixing performance of fixed and fluidized beds of spherical, monodisperse particles confined in micro-channels. In terms of scalar dispersion, beds involving moving particles and those with fixed particles show intriguing differences: dispersion in macroscopic fixed beds was discussed in Levenspiel's monograph (Levenspiel, 1962), where it was demonstrated that an increase of the solids volume fraction increases scalar dispersion. Simulations involving scalar dispersion by mobile particles in relatively dilute suspensions show an opposite trend (Derksen, 2008b): reduction of dispersion towards higher solids volume fractions, where it should be noted that in these simulations the moving particles were not confined by walls, and were one-way coupled (solid-to-fluid only) to the fluid in which the scalar was dissolved.

Our method of research is purely computational: the flow of interstitial liquid in the channel with particles is solved with the lattice-Boltzmann method (Chen and Doolen, 1998; Succi, 2001). Scalar mixing is assessed by solving the convection-diffusion equation of a passive scalar dissolved in the liquid phase with a finite volume scheme, and appropriate boundary conditions at the particles surfaces. Given that laminar flows are considered and that relatively simple geometries are used, the computational approach requires a minimum of modelling. The Navier–Stokes equations are solved directly, and (in the fluidized particle simulations) are fully coupled to the motion of the solid particles: the moving particles constitute no-slip conditions for the interstitial liquid; and the particle motion is the result of hydrodynamic forces induced by the liquid flow. In the moving-particle-simulations, particles undergo hard-sphere collisions that are explicitly resolved.

In applications as the ones considered here that require hardly any modelling, computational simulation is a truly

E-mail address: jos@ualberta.ca.

Received 12 September 2008; Received in revised form 23 October 2008; Accepted 27 October 2008
0263-8762/$ – see front matter © 2008 The Institution of Chemical Engineers. Published by Elsevier B.V. All rights reserved.
doi:10.1016/j.cherd.2008.10.007

Nomenclature

c, c_0	scalar concentration, initial scalar concentration
$c_{z<H/2}$	average scalar exit concentration in half the channel
d_p	particle diameter
$\mathbf{g}$	gravitational acceleration vector
H	channel width
L_b, L_d, L_u	channel portions (bed, downstream, and upstream length, respectively)
$\mathbf{r_p}$	particle center position
$Re_c = u_{in}H/\nu$	channel Reynolds number
$Sc = \nu/\Gamma$	Schmidt number
t	time
T_g	granular temperature
u_{in}	inlet velocity
$\mathbf{v_p}$	particle velocity
v_s	particle settling velocity
x, y, z	spatial coordinate system

Greek symbols

ϕ	solids volume fraction
ν	kinematic viscosity
ρ_s, ρ_l	solid and liquid density
Γ, Γ_e	diffusivity, effective diffusivity
$\mathbf{\Omega_p}$	particle angular velocity

competitive alternative for experimentation. The level of realism that can be reached is very high. On top of that, simulations give direct access to the full data (scalar fields; flow fields; particle positions, velocities, collisions, etc.). Obviously simulations cannot fully replace experimentation in the type of applications discussed here; an appropriate balance between stimulations and experiments builds confidence in simulation results and guides experimental effort.

This paper is organized in the following manner. We first describe the flow systems in terms of their geometry and dimensionless numbers. Then we briefly describe the computational approach. Results comprise the characterization of the mixing performance of the various micro solid–liquid systems investigated, and the liquid–solid fluidization behaviour in narrow channels at low Reynolds numbers. Furthermore, it is shown how design choices (e.g. particle size relative to channel width, channel length, and flow rate) influence mixing performance. Finally we summarize our findings.

1.1. *Channel layouts and flow conditions*

We consider vertically placed channels with square cross-sections (see Fig. 1). At the bottom of the channel we force fluid in by imposing a uniform velocity u_{in} over the cross-sectional area. This velocity, the channel width H and the fluid's viscosity ν define the channel's Reynolds number: $Re_c = u_{in}H/\nu$. In the channel we place uniformly sized spherical particles with diameter d_p. Two situations are being considered. In the first, spheres are placed in random close packing with fixed positions. The bed of particles has a length L_b. Upstream and downstream of the bed the channel is void of particles over length L_u and L_d, respectively (see Fig. 1). In the second situation, the particles are confined to the same space with length L_b. However, they now move freely around within this space. At its lower and upper end the particles collide on an imaginary wall that the fluid passes undisturbed. These boundaries can be viewed as very fine wire meshes (with mesh width much smaller than d_p). The particles are fluidized by the upward liquid flow.

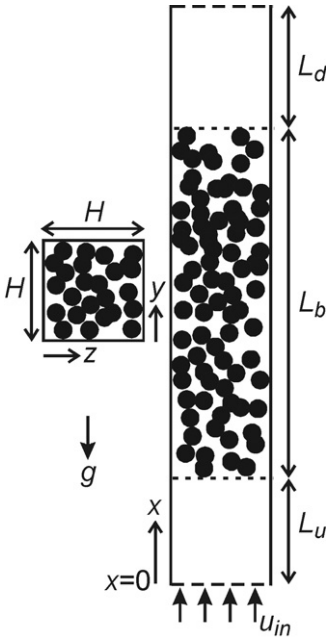

Fig. 1 – Micro-channel flow geometry including definition of the coordinate system. The vector g indicates the direction of gravity and is in the negative *x*-direction.

The main dimensionless numbers governing the liquid–solid system are the solids volume fraction ϕ of the particle bed (with ϕ being defined as the volume occupied by the solids over the part of the channel volume allowed for the particles H^2L_b), the aspects ratios d_p/H and L_b/H, and the solid over fluid density ratio ρ_s/ρ_l. Finally – since we will be considering cases with fluidized particles in vertical channels – gravitational acceleration $\mathbf{g}$ plays a role. It is introduced via the Stokes settling velocity of a single particle in unbounded fluid $v_s = 1/18\,(\rho_s - \rho_l)|\mathbf{g}|/\rho_l \nu\, d_p^2$ as included in the velocity ratio v_s/u_{in}.

Scalar mixing is quantified by solving the convection-diffusion equation for a passive scalar concentration c with scalar diffusivity Γ (and Schmidt number $Sc = \nu/\Gamma$) dissolved in the liquid. The scalar enters fully segregated at the bottom side (at $x = 0$) of the mixer: in half of the inlet cross-section ($z < H/2$), no scalar is added; in the other half of the inlet cross-section ($z > H/2$) we maintain a scalar concentration of $c = c_0$. The scalar release at $x = 0$ only starts when the solid–liquid flow is fully developed; the start of scalar release is denoted with $t = 0$.

To limit our parameter space, two dimensionless groups were set constant throughout the research: $\rho_s/\rho_l = 2.5$ (e.g. solid glass beads in water) and $Sc = 10^3$ (which is a typical Schmidt number for liquid systems).

1.2. *Computational approach*

The lattice-Boltzmann method (LBM) (Chen and Doolen, 1998; Succi, 2001) has been used to solve the fluid flow in the channel and in between the spherical particles. At the inlet ($x = 0$) a uniform velocity u_{in} is imposed; at the outlet (at $x = L_u + L_b + L_d$) we have a zero-axial-gradient condition ($\partial/\partial x = 0$). The chan-

nel walls as well as the spherical particle surfaces are no-slip boundaries. For the fixed bed cases, the fluid velocity at the spherical particle surfaces is zero. In case of mobile particles, fluid and particle motion are fully coupled by demanding that at the surface of each sphere the fluid velocity matches the local velocity of its surface (which is the sum of the linear velocity $\mathbf{v}_p$, and rotation $\boldsymbol{\Omega}_\mathbf{p} \times (\mathbf{r} - \mathbf{r}_\mathbf{p})$ with $\boldsymbol{\Omega}_\mathbf{p}$ the angular velocity of the sphere, $\mathbf{r}_\mathbf{p}$ the center position of the sphere, and $\mathbf{r}$ a point on its surface). In the forcing scheme that is applied here for establishing no-slip at the spherical surfaces this is accomplished by imposing additional forces on the fluid at the surface of the solid sphere. The details of the implementation can be found elsewhere (Goldstein et al., 1993; Derksen and Van den Akker, 1999). The collection of forces representing the no-slip conditions are added up to determine the hydrodynamic force and torque acting on each sphere (action = −reaction). In case of mobile spheres, these are used to evaluate the equations of linear and rotational motion of the spheres. Sphere–sphere and sphere–wall collisions are considered fully elastic and smooth (no friction). In the low Reynolds number/highly viscous flows considered here this is not a drastic assumption since energy is largely dissipated in the liquid anyhow (Derksen and Sundaresan, 2007).

The spatial resolution of the simulations is such that the particle diameter d_p spans 12 lattice spacings. Grid sensitivity of the forcing method in LBM context (Ten Cate et al., 2002; Derksen and Sundaresan, 2007; Derksen, 2008a) has shown that $d_p = 12$ is sufficient resolution.

The dispersion of the passive scalar dissolved in the continuous phase fluid is simulated by numerically solving a convection-diffusion equation for the scalar concentration c. For this an explicit finite volume representation on the same grid as used by the LBM is employed. To limit numerical diffusion, we apply TVD discretization with the Superbee flux limiter for the convective fluxes (Hartmann et al., 2006; Harten, 1983; Sweby, 1984). We step in time according to an Adams-Bashford scheme. We do not allow scalar concentration inside the spherical particles. At the surface of the particles we impose $\partial c/\partial n = 0$. This condition is also applied for assigning concentrations to grid nodes that get uncovered by a moving solid particle. Since particles typically move less than 0.05 times the lattice spacing per time step, an uncovered node always is close to a solid particle interface. We draw the normal out of the particle into the fluid at the position of the uncovered node. By interpolation we determine the concentration on the normal 1 additional grid spacing into the fluid and assign that concentration to the uncovered node. In some situations this cannot be done: it occasionally occurs that a grid node gets uncovered in between two closely spaced particles moving away from each other after a collision. In such cases we assign the average concentration in the direct vicinity to the uncovered grid node, while keeping that vicinity as small as possible. Particles covering and uncovering grid nodes containing concentration information makes the simulations not inherently mass conservative. In practice mass is conserved within 0.5% over the full length of a simulation (the latter being of the order of 5×10^5 time steps, which corresponds to approximately $20(H/u_{in})$).

2. Results

In discussing the results, the focus will be on comparing the mixing performance of fixed and fluidized beds, and on the fluidization characteristics in the narrow and low-Reynolds number beds as used here.

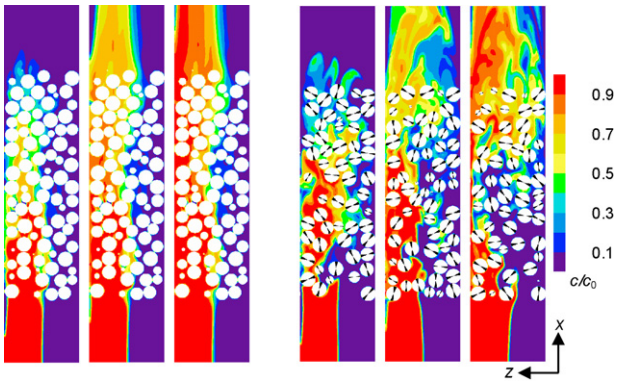

Fig. 2 – Scalar concentration in the center xz-plane at three moments in time ($t = 2, 4, 8 \times H/u_{in}$) after starting the release of the scalar at $x = 0$. Left three panels: fixed bed ($\phi = 0.504$). Right three panels: fluidized bed ($\phi = 0.365$, $v_s/u_{in} = 24$). In both cases $Re_c = 12.2$, $d_p/H = 0.197$, and $L_b/H = 3.28$.

Typical results in terms of evolving concentration fields for a fixed bed and a fluidized bed case are given in Fig. 2. We look at the center cross-section through the channel at three moments after the scalar release. The round disks are the cross-sections of the spheres; all spheres have the same size but are positioned differently with respect to the cross-section. In the fluid bed we keep track of the orientation of the spheres (indicated by the black markers on each sphere); the orientation of the spheres in case of a fixed bed is irrelevant. The thin, horizontal white lines in the panels related to fluidized particles are the boundaries the spheres are confined to. In Fig. 3 are snapshots of the scalar concentration fields in the exit plane for the fixed and fluidized bed, clearly showing that at the exit the scalar field has not completely forgotten its segregated state in which it entered.

The scalar mixing performances of the fixed and fluidized bed are clearly different. The motion of the fluidized particles induces fluid motion that helps in dispersing the scalar. Particle motion induces temporal variation as well as shown in the time series of the cross-sectional average concentration in the exit plane (Fig. 4). A simple way to characterize scalar dispersion is by monitoring at the exit plane how much scalar has reached the "other" side of the channel, i.e. that part of the channel's cross-section where no scalar was injected at the inlet plane. We quantify this with the average scalar concentration over that part of the exit plane with $z < H/2$ (denoted as $c_{z<H/2}$). A value of $c_{z<H/2} = 0$ implies no dispersion at all; a value of $0.5c_0$ implies ideal dispersion since in that case the exit concentration must be virtually uniform. Time series of $c_{z<H/2}$ have been included in Fig. 4. They show a steady-state value of $c_{z<H/2} = 0.139c_0$ for the fixed bed case, and a time-averaged value of $0.291c_0$ (and standard deviation $0.43c_0$) for the fluidized case in quasi-steady-state (reached after $tu_{in}/H \approx 10$).

Increasing the length of the channel helps in better spreading the scalar. In Fig. 5a we show results of three simulations in terms of $c_{z<H/2}$ for three lengths of the reactor; the rest of the conditions are the same for these three cases. The exit concentration $c_{z<H/2}$ increases, albeit marginal for the fixed bed; its standard deviation (for the fluidization cases) decreases with length. The exit concentration $c_{z<H/2}$ can be translated in an effective diffusion (or dispersion) coefficient Γ_e through

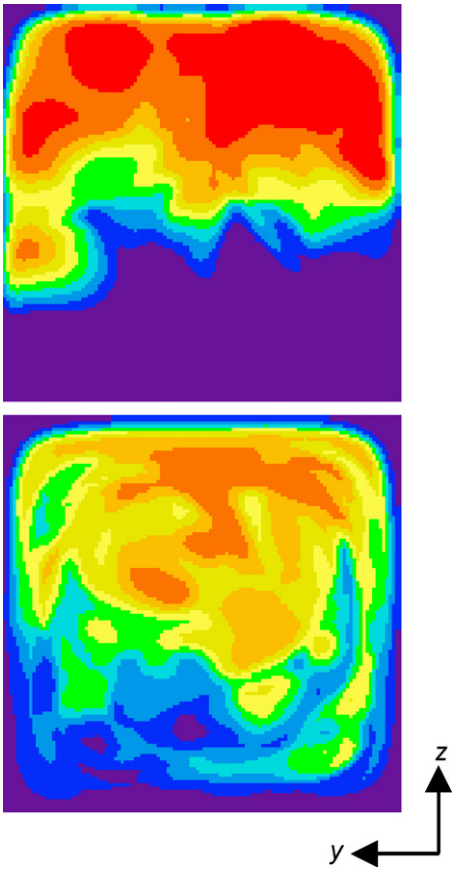

Fig. 3 – Scalar concentration in the exit plane at $t = 8\ H/u_{in}$. Top panel: fixed bed; bottom panel: fluidized bed. Same conditions and color scale as Fig. 2.

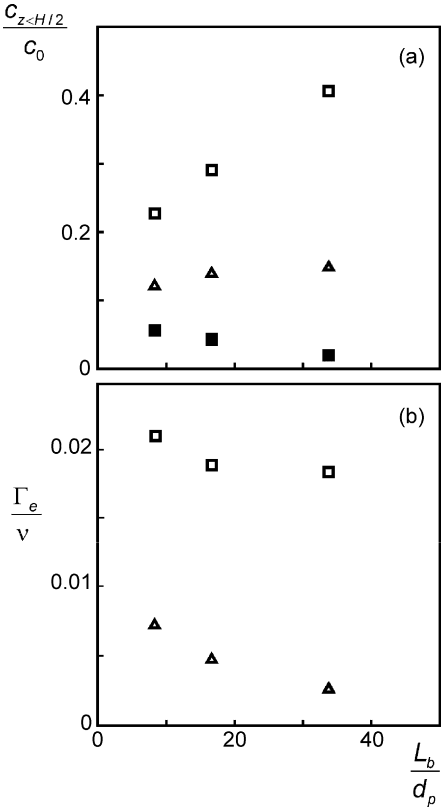

Fig. 5 – Exit concentrations $c_{z<H/2}$ (a), and effective diffusivities (b) as a function of reactor length. The open squares indicate the fluidized bed; the triangles the fixed bed. The filled squares in (a) indicate the RMS of the fluctuations for the fluidized cases.

a simple, one-dimensional diffusion model:

$$\Gamma_e = \frac{1}{4\pi}\left(\frac{c_{z<H/2}}{c_0}\right)^2 \frac{H^2 u_{in}(1-\phi)}{L_b} \quad (1)$$

In the analysis leading to Eq. (1) we use penetration theory to estimate the mass transfer across the $z = H/2$ plane. The mass transfer coefficient then is $\bar{k} = 2\sqrt{\pi\,\Gamma_e/t_e}$ with t_e the time a fluid package spends on average in the bed: $t_e = L_b(1-\phi)/u_{in}$.

The results in Fig. 5b show that for the fluidized system Γ_e only weakly depends on L_b, giving credit to the simple diffusion model. For the fixed beds the effective diffusivity varies much stronger with length making the one-dimensional model less appropriate for such systems. In any case, the diffusivity brought about by the fluidized particles is generally four times higher than for fixed beds. Fixed beds in turn have a roughly five times higher diffusivity than the no-particles situation where the ratio of (molecular) diffusivity over viscosity is $1/Sc = 0.001$.

From now on, the mixing performance will be expressed in terms of Γ_e, calculated from Eq. (1) and (in quasi-steady-state) the time-averaged values of $c_{z<H/2}$. Given the relatively poor dispersion capacity of the laminar fixed bed, the remainder of this paper will focus on low Reynolds number *fluidized* beds.

There are many choices to be made in designing a micro-fluidized bed mixer. We will discuss three of them here:

- *The flow rate through the bed*: it has a lower bound for which the particles do not get fluidized, and an upper bound for which the particles get blown against the upper grating; in both cases the bed approaches a fixed state with apparently bad consequences for its mixing capacity.
- The size of the particles relative to the channel width H.
- The solids volume fraction ϕ.

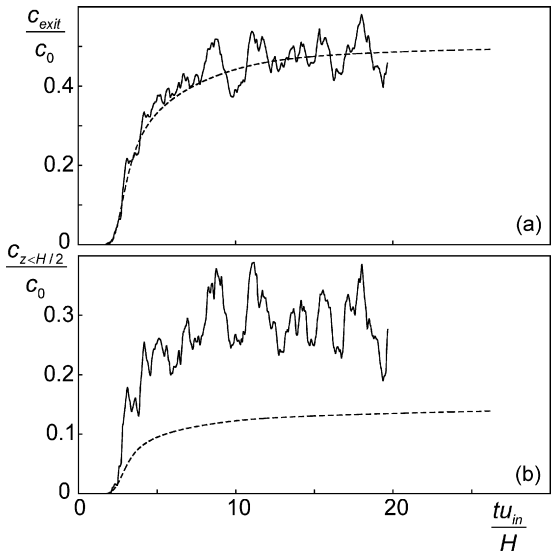

Fig. 4 – Time series of the average concentration in the exit plane (a), and lower portion of the exit plane (with $z < H/2$) (b) for the fixed bed (dashed line) and fluidized bed (solid line) cases as depicted and defined in Fig. 2.

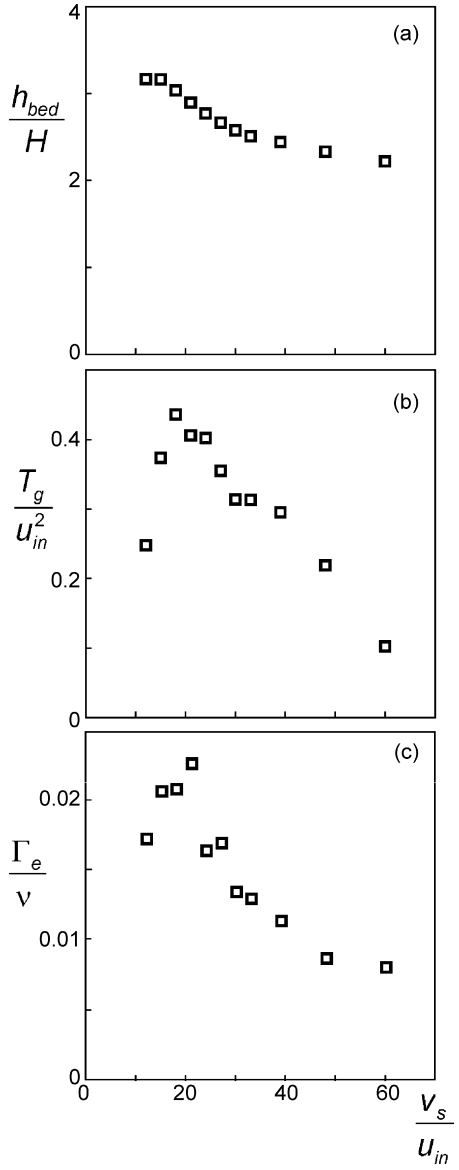

Fig. 6 – Fluidized bed height (a), granular temperature (b), and effective diffusion coefficient (c) as a function of the ratio v_s/u_{in}. $Re_c = 12.2$, $\phi = 0.365$, $d_p/H = 0.197$, $L_b/H = 3.28$.

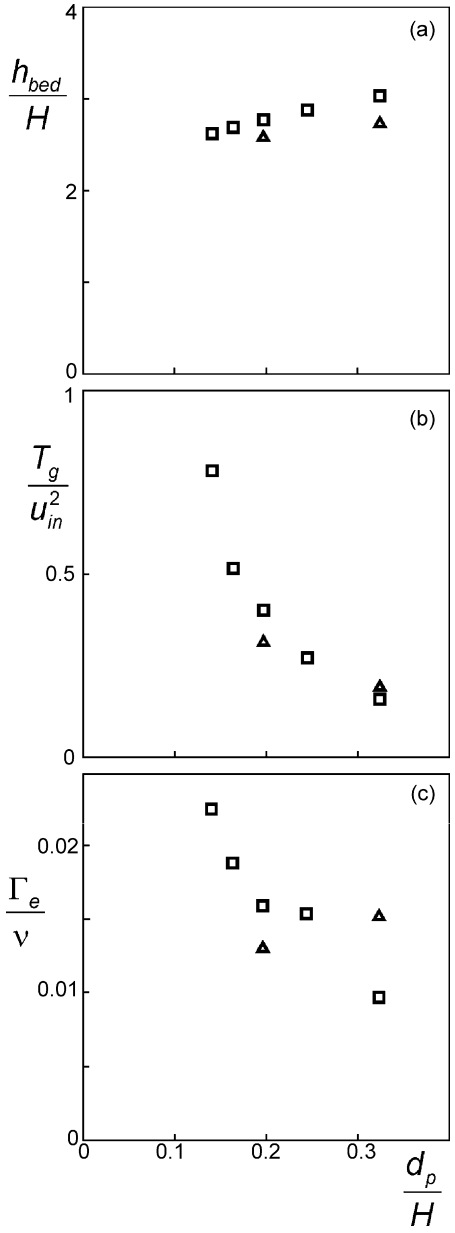

Fig. 7 – Fluidized bed height (a), granular temperature (b), and effective diffusion coefficient (c) as a function of particle diameter d_p relative to bed width H. Squares relate to $v_s/u_{in} = 24$, triangles to $v_s/u_{in} = 30$. $Re_c = 12.2$, $\phi = 0.365$, and $L_b/H = 3.28$.

In general, the flow rate ($u_{in}H^2$) and also the ratio H/d_p may have consequences for the channel's Reynolds number Re_c. With respect to the latter: for a given channel size, smaller particles require a lower flow rate for fluidization. With the same liquid properties this would imply a lower Re_c. However, in order to single out the effect of fluidization properties (bed expansion, granular temperature) on scalar mixing, the simulations were set up such that Re_c was fixed to 12.2. This was achieved by adjusting the liquid's viscosity.

As the relevant dimensionless parameter controlling the flow rate we consider the ratio of the settling velocity of the particles over the inlet velocity v_s/u_{in}. In Fig. 6 we show how the fluidized bed characteristics depend on this velocity ratio. In terms of the bed height (which is defined as the time-average of the average x-position of the top eight particles at any moment in the bed) we clearly see an upper limit (particles pushed against the upper grating for low v_s/u_{in}) and a lower limit (particles forming an almost fixed bed supported by the lower grating for high v_s/u_{in}). This reflects in the granular temperature ($T_g = 1/2(\overline{\mathbf{u}_s' \cdot \mathbf{u}_s'})$ with $\mathbf{u}_s'$ the fluctuating part of the solids velocity)[1] going through a maximum at $v_s/u_{in} \approx 20$. As a consequence of this, the effective diffusivity goes through a maximum at a nearby v_s/u_{in} value ($v_s/u_{in} \approx 22$); the higher the granular temperature, the better the liquid is stirred by the particles.

The mixing performance of the bed clearly depends on the particle size relative to the channel width; see Fig. 7. Smaller particles generally show higher effective diffusion coefficients. It should be noted that at the high end of the particle size, the particles are blown against the upper grating if $v_s/u_{in} \approx 24$. Increasing that value to 30 prevents this and strongly increases Γ_e for the big particles (see the triangular symbol in Fig. 7c at $d_p/H = 0.32$).

[1] Which in this specific case is the same as the instantaneous particle velocity given the average particle velocity being zero.

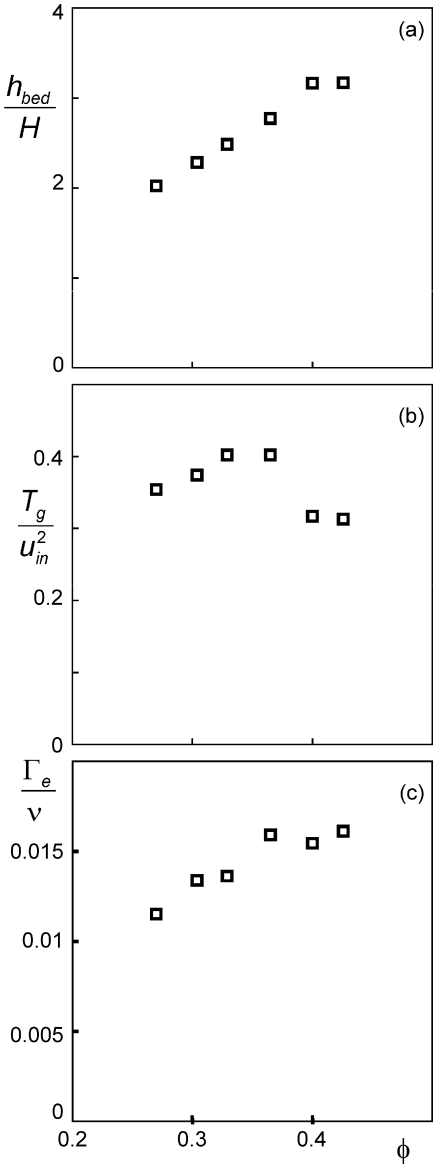

Fig. 8 – Fluidized bed height (a), granular temperature (b), and effective diffusion coefficient (c) as a function ϕ with further $v_s/u_{in} = 24$, $Re_c = 12.2$, $d_p/H = 0.197$, and $L_b/H = 3.28$.

Finally the effect of the overall solids volume fraction (as defined in Section 1.1) on fluidization and mixing is displayed in Fig. 8. In the range of solids volume fractions investigated, we observe a slight but continuous increase of the effective diffusion coefficient with increasing ϕ. At the higher end this trend levels off as the mobility of the particles decreases (reflected in e.g. a decrease in granular temperature). The trend observed here is opposite to the one observed in the simulations by Derksen (2008b) for unconfined, granular particles. There a decrease of effective diffusivity was observed with increasing solids volume fraction. Two effects could explain this potential controversy: (1) In Derksen (2008b) the granular temperature and domain size were imposed and constant for simulations and therefore decoupled from the solids volume fractions; in this paper the granular temperature and the bed height vary, partly as a result of the varying solids volume fraction (Fig. 8a and b). (2) In the present work the particles are confined by walls, limiting their mean-free path as opposed to the unconfined particles (fully periodic boundary conditions) in Derksen (2008b).

3. Summary

In this paper we discussed the mixing in narrow (laminar) channels of a passive scalar dissolved in a liquid in the presence of fixed and fluidized spherical, solid particles. The method of research was purely computational: the liquid flow, the solid particle motion (in case of fluidized beds), and the scalar transport were all directly resolved by the numerical methodology. Fluid flow was solved with the lattice-Boltzmann method; solid particle motion was directly coupled to this method with particles undergoing hard-sphere collisions; passive scalar transport was simulated with a finite volume scheme on the same grid as used for the LBM. The computational method did not involve ad hoc models; the governing equations were directly solved.

Compared to fixed beds, the mixing performance (quantified in terms of an effective diffusion coefficient) of fluidized beds was much better, and the focus of the paper is therefore on the latter.

We have been able to relate the mixing performance of the fluidized mixing device in terms of an effective diffusion coefficient (scaled with the liquid's kinematic viscosity) with a number of dimensionless process parameters. The sensitivities observed are partly typical for the specific geometry (with confined space for the particles), partly more universal (e.g. in terms of the impact of solids volume fraction or relative particle size on effective diffusivity). An important finding was that the micro-channel mixing device is operable in a broad range of superficial liquid velocities. As shown (Fig. 6c) it mixes much better than a fixed bed reactor in the investigated range of settling velocity over superficial velocity. Furthermore, finer particles mix better than coarser particles, and increasing the solids volume fraction also slightly helps in mixing the scalar. The latter against the "cost" of a higher pressure drop.

References

Andersson, H., van der Wijngaart, W., Enoksson, P. and Stemme, G., 2000, Micromachined flow-through filter-chamber for chemical reactions on beads. Sensors Actuat. B, 67: 203–208.

Chen, S. and Doolen, G.D., 1998, Lattice Boltzmann method for fluid flows. Annu. Rev. Fluid Mech., 30: 329–364.

Derksen, J.J. and Van den Akker, H.E.A., 1999, Large eddy simulations on the flow driven by a Rushton turbine. AIChE J., 45: 209–221.

Derksen, J.J. and Sundaresan, S., 2007, Direct numerical simulations of dense suspensions: wave instabilities in liquid-fluidized beds. J. Fluid Mech., 587: 303–336.

Derksen, J.J., 2008, Flow induced forces in sphere doublets. J. Fluid Mech., 608: 337–356.

Derksen, J.J., 2008, Scalar mixing by granular particles. AIChE J., 54: 1741–1747.

Djenida, L. and Moghtaderi, B., 2006, Numerical investigation of laminar mixing in a coaxial microreactor. J. Fluid Mech., 568: 223–242.

Goldstein, D., Handler, R. and Sirovich, L., 1993, Modeling a no-slip flow boundary with an external force field. J. Comp. Phys., 105: 354–366.

Harten, A., 1983, High resolution schemes for hyperbolic conservation laws. J. Comp. Phys., 49: 357–393.

Hartmann, H., Derksen, J.J. and Van den Akker, H.E.A., 2006, Mixing times in a turbulent stirred tank by means of LES. AIChE J., 52: 3696–3706.

Johnson, B.K. and Prud'homme, R.K., 2003, Chemical processing and micromixing in confined impinging jets. AIChE J., 49: 2264–2282.

Levenspiel, O., (1962). *Chemical Reaction Engineering* (2nd ed.). (Wiley, New York).

Roelands, M., Derksen, J., Ter Horst, J., Kramer, H. and Jansens, P., 2003, An analysis of mixing in a typical experimental setup to measure nucleation rates of precipitation processes. Chem. Eng. Tech., 26: 296–302.

Succi, S., (2001). *The Lattice Boltzmann Equation for Fluid Dynamics and Beyond*. (Clarondon Press, Oxford).

Sweby, P.K., 1984, High resolution schemes using flux limiters for hyperbolic conservation laws. SIAM J. Num. Anal., 21: 995–1011.

Ten Cate, A., Nieuwstad, C.H., Derksen, J.J. and Van den Akker, H.E.A., 2002, Particle imaging velocimetry experiments and lattice-Boltzmann simulations on a single sphere settling under gravity. Phys. Fluids, 14: 4012–4025.